Two- and One-Dimensional Honeycomb Structures of Silicon and Germanium

S. Cahangirov,[1] M. Topsakal,[1] E. Aktürk,[1] H. Şahin,[1] and S. Ciraci[1,2,*]

[1]*UNAM-Institute of Materials Science and Nanotechnology, Bilkent University, Ankara 06800, Turkey*

[2]*Department of Physics, Bilkent University, Ankara 06800, Turkey*

(Received 27 November 2008; published 12 June 2009)

First-principles calculations of structure optimization, phonon modes, and finite temperature molecular dynamics predict that silicon and germanium can have stable, two-dimensional, low-buckled, honeycomb structures. Similar to graphene, these puckered structures are ambipolar and their charge carriers can behave like a massless Dirac fermion due to their π and π^* bands which are crossed linearly at the Fermi level. In addition to these fundamental properties, bare and hydrogen passivated nanoribbons of Si and Ge show remarkable electronic and magnetic properties, which are size and orientation dependent. These properties offer interesting alternatives for the engineering of diverse nanodevices.

DOI: 10.1103/PhysRevLett.102.236804 PACS numbers: 73.22.−f, 61.48.De, 63.22.−m

The unusual electronic properties of graphene, which is derived from its planar honeycomb structure, lead to charge carriers resembling massless Dirac fermions [1]. Recent synthesis of graphene [2–4] has demonstrated that this truly two-dimensional (2D) structure is stable and has introduced novel concepts [2,5,6]. Not only have the fundamental properties of 2D graphene been revealed, but also the interesting size and geometry dependent electronic and magnetic properties of their quasi-1D nanoribbons [7,8] have been demonstrated. While the research interest in graphene and its ribbons is growing rapidly, one has started to question whether the other group IV elements in the periodic table, such as Si and Ge, have a stable honeycomb structure [9,10]. Even before the synthesis of isolated graphene, *ab initio* studies based on the minimization of the total energy has revealed that a buckled honeycomb structure of Si can exist [9,10].

In this Letter, based on state-of-the-art structure optimization, phonon dispersion, and *ab initio* finite temperature molecular dynamics calculations within density functional theory (DFT) [11] we show that the low-buckled honeycomb structures of Si and Ge can be stable. Their band structures show linear band crossing at the Fermi level and thus have Dirac points at the K and K' points of the hexagonal Brillouin zone (BZ), even for puckered structure. These results are somehow unexpected but may have important consequences. For example, the bands display an ambipolar character and the charge carriers behave like massless Dirac fermions in a small energy range around the Fermi level E_F. Even more remarkable is that the armchair and zigzag nanoribbons of Si and Ge can exist and display unusual properties which are crucial for future device applications.

Calculated variation of the binding energy of the relaxed honeycomb structure of Si and Ge as a function of the lattice constant is presented in Fig. 1. Here planar (PL), low-buckled (LB), and high-buckled (HB) honeycomb structures correspond to distinct minima. The PL honeycomb structure is the least energetic configuration and is not stable. The important question to be addressed is whether these puckered LB and HB geometries correspond to real local minima in the Born-Oppenheimer surface.

PL structure of Si and Ge have phonon modes, which have imaginary frequencies in BZ. For the minimum energy PL structure of Si, optical and acoustical branches

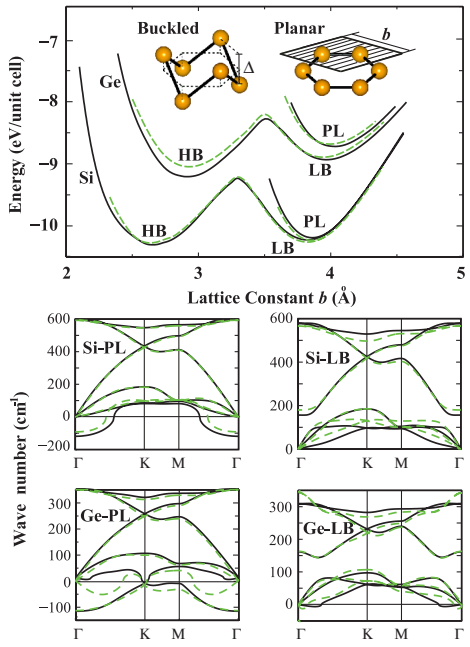

FIG. 1 (color online). Upper panel: Energy versus hexagonal lattice constant of 2D Si and Ge are calculated for various honeycomb structures. Black (dark) and dashed green (dashed light) curves of energy are calculated by LDA using PAW potential and ultrasoft pseudopotentials, respectively. Planar and buckled geometries together with buckling distance Δ and lattice constant of the hexagonal primitive unit cell, b are shown by inset. Lower panels: Phonon dispersion curves obtained by force-constant and linear response theory are presented by black (dark) and dashed green (dashed light) curves, respectively.

 © 2009 The American Physical Society

hybridize and one optical (ZO) branch is lowered into acoustical frequencies and have imaginary frequencies along the Γ-K direction of BZ. The situation for PL Ge structure is even more dramatic with one acoustical and one optical branch having imaginary frequencies. As for HB honeycomb structures of Si and Ge with a buckling of $\Delta_{\mathrm{HB}} \approx 2$ Å, they have also imaginary phonon frequencies for a large portion of BZ. Moreover, structure optimization of HB structure on the (2×2) supercell results in an instability with a tendency towards clustering. Clearly, the unstable HB structure does not correspond to a real local minimum; it can occur only under the constraint of the (1×1) hexagonal lattice.

The phonon dispersion curves in Fig. 1 indicate that 2D periodic LB honeycomb structure of Si is stable. With an equilibrium buckling $\Delta_{\mathrm{LB}} = 0.44$ Å, its optical and acoustical branches are well separated and all branches have positive frequency. Two acoustical branches are linear as $\mathbf{k} \rightarrow 0$. Whereas the transverse branch displays a quadratic dispersion near Γ point, since the force constants related with the transverse motion of atoms decay rapidly [12]. The phonon dispersion curves of 2D periodic LB structure of Ge having a buckling of $\Delta_{\mathrm{LB}} = 0.64$ Å are similar to those of Si, except the frequencies of Ge are almost halved due to relatively smaller force constants. The transverse acoustical phonon branch has imaginary frequencies near the Γ point. This may be interpreted as LB structure of Ge can be unstable if the wavelength of this particular mode $\lambda > 3b$ ($7b$ according to phonon dispersion curves calculated using DFPT [11]), whereas its flakes can be stable. In fact, the structure optimization on the $(l \times l)$ supercells (where for $l = 2$–8 atoms are displaced along random directions from their optimized positions and subsequently the structure is relaxed) results in the atomic configuration with periodic rippling for $l > 3$. The stability of LB structures of Si and Ge are further tested by extensive *ab initio* finite temperature molecular dynamics calculations using time steps of $\delta t = 2 \times 10^{-15}$ seconds. In these calculations the (4×4) supercell is used to lift the constraint of (1×1) cell. Periodic 2D LB structure of Si (Ge) is not destroyed by raising the temperature from $T = 0$ to 1000 K (800 K) in 100 steps, and holding it at $T = 1000$ K (800 K) for 10 picoseconds (ps). A finite size, large hexagonal LB flake of Si (Ge) with hydrogen passivated edge atoms is not destroyed upon raising its temperature from 0 to 1000 K (800 K) in 100 steps and holding it for more than 3 ps.

We believe that the present analysis together with calculated phonon dispersion curves provides a stringent test for the stability of LB honeycomb structure of both Si and Ge. In this respect, LB structures of Si and Ge appear to be a contrast to 2D C and BN forming only stable planar honeycomb structure [13]. The situation with three different minima corresponding to PL, LB, and HB geometries of 2D Si and Ge in Fig. 1 is reminiscent of those of 1D atomic chains. Earlier, it has been shown that while several elements and III-V compounds form linear, wide-angle (i.e., LB) and low-angle (i.e., HB) atomic chains [14,15], only C and BN form stable linear atomic chains [15,16]. That C and BN form linear 1D atomic chains and 2D planar honeycomb structures arises from the strong π bonding. Despite the weakened π bonding, the stability of Si and Ge LB structures is maintained by puckering induced dehybridization. As a result, the perpendicular p_z orbital, which forms π bonding and hence π and π^* bands, combines with the s orbital. Relevant lattice parameters and cohesive energies of LB Si and Ge honeycomb structures are given in Table I. Different potentials (PAW or ultrasoft pseudopotential) [11] yielded values which differ only 1%.

The calculated electronic band structures and corresponding density of states (DOS) of LB Si and Ge are presented in Fig. 2. For the sake of comparison bands for unstable planar and HB structures are also given. Two-dimensional HB Si and Ge are metallic. The bands of PL and LB structures are similar except that specific degeneracies split due to lowering of point group rotation symmetry from C_6 in PL geometry to C_3 in LB geometry. Similar to graphene, π- and π^* bands of LB Si crossing at K and K' points at E_F are semimetallic. For PL Ge, since the s-like lowest conduction band of planar Ge dips into the Fermi level, π and π^* bands cross at K and K' points above the Fermi level. Therefore, PL structure of Ge is metallic. Upon a structural transformation from PL to LB structure, the crossing point of the π and π^* bands of Ge shifts to Fermi level. At the end, LB structure of Ge becomes also semimetallic. Around the crossing point, these bands are linear. This behavior of bands, in turn, attributes a massless Dirac fermion character to the charge carriers. Interestingly, by neglecting the second and higher order terms with respect to q^2, the Fermi velocity is estimated to be $v_F \sim 10^6$ m/s for both Si and Ge by fitting the π and π^* bands at $\mathbf{k} = \mathbf{K} + \mathbf{q}$ to the expression

$$v_F \simeq E(\mathbf{q})/\hbar|\mathbf{q}|. \quad (1)$$

We note that v_F calculated for LB honeycomb structures of Si and Ge are rather high and close to that calculated for graphene using the tight-binding bands. In addition, because of the electron-hole symmetry at K and K' points of BZ, LB Si and Ge are ambipolar for $E(\mathbf{q}) = E_F \pm \epsilon$,

TABLE I. Binding energy and structural parameters calculated for the bulk and 2D Si and Ge crystals. a_{bulk} [in Å], $E_{c,\mathrm{bulk}}$ [in eV per atom], Δ_{HB} [in Å], Δ_{LB}, b_{LB}, d_{LB}, and $E_{c,\mathrm{LB}}$, respectively, stand for bulk cubic lattice constant, bulk cohesive energy, high-buckling distance, low-buckling distance, hexagonal lattice constant of 2D LB honeycomb structure, corresponding nearest neighbor distance, and corresponding cohesive energy.

	a_{bulk}	$E_{c,\mathrm{bulk}}$	Δ_{HB}	Δ_{LB}	b_{LB}	d_{LB}	$E_{c,\mathrm{LB}}$
Si	5.41	5.92	2.13	0.44	3.83	2.25	5.16
Ge	5.64	5.14	2.23	0.64	3.97	2.38	4.15

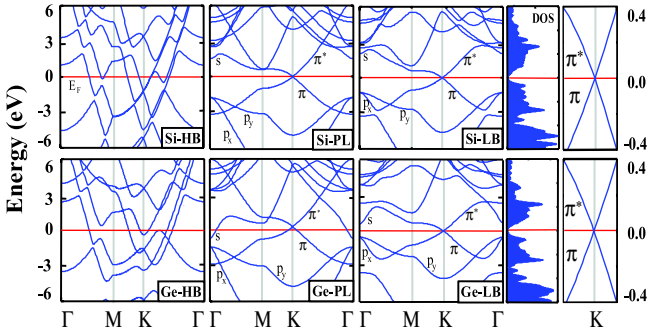

FIG. 2 (color online). Energy band structure of Si and Ge are calculated for high-buckled (HB), planar (PL), and low-buckled (LB) structures. For LB structure the density of states (DOS) is also presented. The crossing of the π and π^* bands at K and K' points of BZ is amplified to show that they are linear near the cross section point. Zero of energy is set at the Fermi level, E_F. s, $p_{x,y}$ orbital character of bands are indicated.

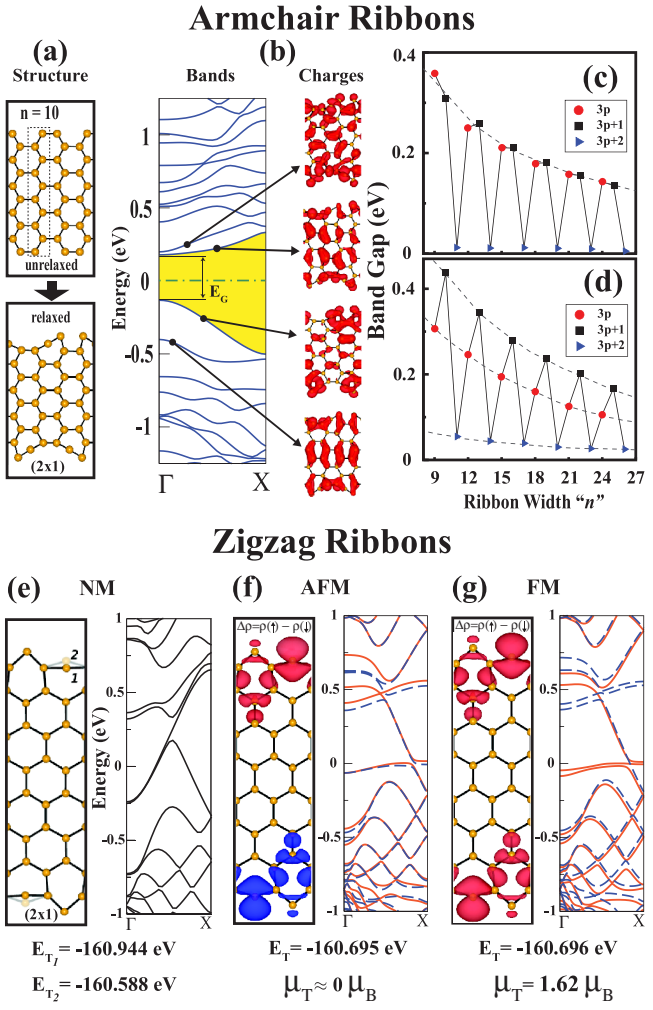

FIG. 3 (color online). Ideal and relaxed atomic structure displaying a (2×1) asymmetric dimerlike reconstruction (a); electronic energy bands and isosurface charge density of selected states (b); variation of band gap E_G with the width n of bare Si armchair nanoribbons (c); and similar variation of E_G for the hydrogen saturated nanoribbons showing oscillations depending on whether $n = 3p$, $3p + 1$ or $3p + 2$ (p being an integer) (d). Bare Si zigzag nanoribbons showing two different (2×1) reconstruction geometries [18] indicated by "1" and "2" and the band structure of metallic nonmagnetic (NM) ground state corresponding to "1" (e). Isosurfaces of spin density difference $[\Delta\rho = \rho^{\uparrow} - \rho^{\downarrow}]$ for spin-up (red or light) and spin-down (blue or dark) states in different magnetic excited states together with spin-up (solid red or light) and spin-down (dashed blue or dark) bands: Antiferromagnetic (AFM) state (f); and ferromagnetic (FM) state (g) together with their calculated total energies and magnetic moments. Zero of the energy is set to E_F.

ϵ being small. The ambipolar effect and high v_F of LB Si and Ge are remarkable properties.

While LB crystals of Si and Ge are of fundamental importance, any application involving these materials requires only a small piece of them or a flake, but not an infinite size. In this respect, their ribbons of nanometer scale with well-defined shape may be crucial for device applications. Whether nanoribbons of Si and Ge show behaviors similar to graphene is the next question to be answered. Here we consider Si and Ge armchair and zigzag nanoribbons of different widths, in terms of the number of Si or Ge atoms n forming a continuous chain between two edges. The ribbons having width $n > 7$, $\sim$1 nm, preserve their LB honeycomb structure upon structure relaxation. The value of the buckling decreases near the edges. Both of their edges undergo a (2×1) reconstruction, which is different for different orientation; whereas the reconstruction disappears when the dangling bonds at the edges are terminated by hydrogen atoms.

In Fig. 3(a), we show the minimum energy reconstruction pattern of $n = 10$ armchair nanoribbons among four other (2×1) patterns. Si armchair nanoribbons are nonmagnetic semiconductors with band gaps relatively smaller than those of graphene. Generally, owing to quantum confinement effect the band gap E_G increases with decreasing width n. However, similar to graphene, the variation of E_G with n shows an oscillatory (or family) behavior. For example, if $n = 3p + 2$ (p being an integer), E_G is very small, but it is large for $n = 3p$ and $n = 3p + 1$. Upon the saturation of dangling bonds with hydrogen, the value of the band gap increases for small n, but continues to show "oscillatory behavior." In this case also E_G is still small for $n = 3p + 2$. Similar oscillatory behavior is also calculated for Ge armchair nanoribbons. We note that the DFT may underestimate the calculated band gaps. The variation of the band gap with n is an important property, which may lead to formation of quantum dot or multiple quantum wells through the width modulation [17].

We performed spin-dependent total energy and electronic structure calculations for bare and hydrogen terminated zigzag nanoribbons. In the (2×1) reconstruction of bare zigzag nanoribbons in Fig. 3(e), one Si atom at the

edge is pushed down while the adjacent atom is raised. This situation is reminiscent of the (2×1) reconstruction of Si(111) surface pointed out earlier by Haneman [18]. In Fig. 3(e) one distinguishes, however, out-of-plane and in-plane reconstruction geometries indicated by "1" and "2", respectively. We found that the out-of-plane (2×1) reconstruction geometry has a nonmagnetic (NM), metallic ground state. However, metallic antiferromagnetic (AFM) and ferromagnetic (FM) states in Figs. 3(f) and 3(g), respectively, are excited states. This situation is, however, reversed upon the termination of dangling bonds by hydrogen; namely, magnetic states have lower energies than the NM state. The analysis of the difference charge density, $\Delta\rho = \rho^{\uparrow} - \rho^{\downarrow}$ in Figs. 3(f) and 3(g) indicates that the AFM and FM states have almost equal energies, the FM state being 1 meV more energetic. This energy difference between AFM and FM states, which is within the accuracy limits of DFT and hence is not decisive, is, however reversed if noncollinear calculations including spin-orbit interaction are performed. In the AFM case, the edge states have opposite spins and approximately zero magnetic moment in the unit cell. On the other hand, the FM state has magnetic moment of $1.62\mu_B$. In both AFM and FM state in Fig. 3, the lowered edge Si atoms have larger magnetic moment, since each raised edge atom donates electrons to adjacent lowered edge atoms.

In conclusion, calculations based on DFT show that Si and Ge can remain stable in LB honeycomb structure, which attribute them important properties similar to graphene. Armchair and zigzag nanoribbons of LB Si and Ge in honeycomb structure exhibit electronic and magnetic properties, which depend strongly on their size and geometry. The electronic properties of these nanoribbons undergo dramatic change depending whether their edges are passivated by hydrogen. These properties of Si and Ge nanoribbons can be used for diverse device applications. Further to the predictions of the present study, recent work by Nakano [19] *et al.* achieving the soft synthesis of single Si monolayer sheet on a substrate holds the promise for the synthesis of Si and Ge nanoribbons having honeycomb structures.

We acknowledge stimulating discussions with Can Ataca. Part of the computations have been carried out by using UYBHM at Istanbul Technical University through a grant (No. 2-024-2007).

*ciraci@fen.bilkent.edu.tr

[1] P. R. Wallace, Phys. Rev. **71**, 622 (1947).
[2] K. S. Novoselov *et al.*, Nature (London) **438**, 197 (2005).
[3] Y. Zhang *et al.*, Nature (London) **438**, 201 (2005).
[4] C. Berger *et al.*, Science **312**, 1191 (2006).
[5] M. I. Katsnelson *et al.*, Nature Phys. **2**, 620 (2006).
[6] A. K. Geim and K. S. Novoselov, Nature Mater. **6**, 183 (2007).
[7] Numerous studies have been carried out on the electronic structure of armchair and zigzag graphene ribbons. See, for example, M. Fujita *et al.*, J. Phys. Soc. Jpn. **65**, 1920 (1996); V. Barone, O. Hod, and G. E. Scuseria, Nano Lett. **6**, 2748 (2006); Y.-W. Son, M. L. Cohen, and S. G. Louie, Phys. Rev. Lett. **97**, 216803 (2006); Nature (London) **444**, 347 (2006); M. Y. Han *et al.*, Phys. Rev. Lett. **98**, 206805 (2007).
[8] X. Li *et al.*, Science **319**, 1229 (2008); X. Wang *et al.*, Phys. Rev. Lett. **100**, 206803 (2008).
[9] K. Takeda and K. Shiraishi, Phys. Rev. B **50**, 14 916 (1994).
[10] E. Durgun, S. Tongay, and S. Ciraci, Phys. Rev. B **72**, 075420 (2005); similar analysis has been done on Si nanotubes M. Zhang *et al.*, Chem. Phys. Lett. **379**, 81 (2003).
[11] We have performed first-principles spin-polarized and spin-unpolarized plane-wave calculations within local density approximation (LDA) [D. M. Ceperley and B. J. Alder, Phys. Rev. Lett. **45**, 566 (1980)] using PAW potentials [P. E. Blöchl, Phys. Rev. B **50**, 17 953 (1994)] as well as ultrasoft pseudopotentials [D. Vanderbilt, Phys. Rev. B **41**, 7892 (1990)]. All structures have been treated within supercell geometry using the periodic boundary conditions. A plane-wave basis set with kinetic energy cutoff of 500 eV is used. In the self-consistent potential and total energy calculations the BZ is sampled by $(25 \times 25 \times 1)$ and $(25 \times 1 \times 1)$ special **k** points for 2D and 1D systems. This sampling is scaled according to the size of superlattices. All atomic positions and lattice constants are optimized by using the conjugate gradient method where total energy and atomic forces are minimized. The convergence for energy is chosen as 10^{-5} eV between two steps, and the maximum force allowed on each atom is less than 10^{-4} eV/Å. Maximum pressure on the lattice has been lowered down to 0.1 kbar. Numerical plane-wave calculations have been performed by using VASP package [G. Kresse and J. Hafner, Phys. Rev. B **47**, 558 (1993); G. Kresse and J. Furthmüller, *ibid.* **54**, 11 169 (1996)] with PAW potentials and all calculations have been repeated by PWSCF package [S. Baroni, A. Del Corso, S. Girancoli, and P. Giannozzi, http:/www.pwscf.org/] using ultrasoft pseudopotentials. Phonon dispersion curves obtained using both the force-constant method with forces calculated by VASP and the density functional perturbation theory (DFPT) using plane-wave methods as implemented in PWSCF software.
[12] F. Liu *et al.*, Phys. Rev. B **76**, 064120 (2007).
[13] We note the tendency that BN, SiC, AlN, GaN form planar honeycomb structure, while some of III-V and II-VI compounds are buckled.
[14] P. Sen *et al.*, Phys. Rev. B **64**, 195420 (2001).
[15] R. T. Senger *et al.*, Phys. Rev. B **72**, 075419 (2005).
[16] S. Tongay *et al.*, Phys. Rev. Lett. **93**, 136404 (2004).
[17] H. Sevinçli, M. Topsakal, and S. Ciraci, Phys. Rev. B **78**, 245402 (2008).
[18] D. Haneman, Phys. Rev. **170**, 705 (1968).
[19] H. Nakano *et al.*, Angew. Chem. **118**, 6451 (2006).